Ultrasound assisted the green synthesis of 2-amino-4*H*-chromene derivatives catalyzed by Fe_3O_4-functionalized nanoparticles with chitosan as a novel and reusable magnetic catalyst

Javad safari, Leila javadian

PII: S1350-4177(14)00050-9
DOI: http://dx.doi.org/10.1016/j.ultsonch.2014.02.002
Reference: ULTSON 2512

To appear in: *Ultrasonics Sonochemistry*

Received Date: 21 October 2013
Revised Date: 1 February 2014
Accepted Date: 2 February 2014

Please cite this article as: J. safari, L. javadian, Ultrasound assisted the green synthesis of 2-amino-4*H*-chromene derivatives catalyzed by Fe_3O_4-functionalized nanoparticles with chitosan as a novel and reusable magnetic catalyst, *Ultrasonics Sonochemistry* (2014), doi: http://dx.doi.org/10.1016/j.ultsonch.2014.02.002

Ultrasound assisted the green synthesis of 2-amino-4*H*-chromene derivatives catalyzed by Fe_3O_4-functionalized nanoparticles with chitosan as a novel and reusable magnetic catalyst

Javad safari[a,*] and Leila javadian[a]

[a]Laboratory of Organic Chemistry Research, Department of Organic Chemistry, College of Chemistry, University of Kashan, P. O. Box: 87317-51167, Kashan, I.R.Iran

E-mail address: Safari@kashanu.ac.ir

Abstract. Fe_3O_4 nanoparticles were prepared by chemical coprecipitation method. Subsequently immobilization of chitosan on Fe_3O_4 nanoparticles was accompllished and afforted magnetic Fe_3O_4-chitosan nanoparticles. Synthesized nanoparticles was found to be a magnetic and heterogenious catalyst for an one-pot and efficient synthesis of 2-amino-4*H*-chromenes by condensation of aldehydes with malononitrile and resorcinol under ultrasound irradiation as an ecofriendly method. This convenient procedure allowed us to achieve products under ultrasound irradiation in short time and excellent yield without using of harmful catalyst. The present method will permit a further increase of the diversity within the 2-amino-4*H*-chromene family.

Keywords: Ultrasound irradiation, Fe_3O_4 nanoparticles, Fe_3O_4-chitosan nanoparticles, 2-Amino-4*H*-chromene, Magnetic catalyst, Green catalyst

1. Introduction

In recent decades, iron oxide nanoparticles have been received increasing attention due to their fundamental properties and applications in the several fileds such as catalysts, sensors, high density magnetic recording media and clinical uses [1]. Surface functionalized iron oxide magnetic nanoparticles are a class of functional materials, which have been used in catalysis and biotechnology [2-7]. These hybrid nanoparticles are composed of several components and can exhibit the properties of different component in the same structure [8,9]. The modification of Fe_3O_4 nanoparticles have been carried out by various materials such as precious metals, carbon, silica and biopolymers [10,11]. Biopolymers such as chitosan have been applied as support in many heterogeneous catalytic systems [12]. Chitosan is a natural,

biodegradable and biocompatable polymer has shown extensive range of application. Chitosan contains both primary and secondary hydroxyl groups and amino groups. Therefore, it can activate the electrophilic and nucleophilic compounds by hydrogen bonding and lone pairs [13] (Scheme 1). These requirement are exist in the reaction of aldehyde resorcinol and malononitrile for the synthesis of 2-amino-4*H*-chromenes.

< Scheme1>

2-amino-4*H*-chromenes are of particular utility as they belong to privileged medicinal scaffolds serving for generation of small-molecule ligands with highly pronounced anticoagulant-, diuretic-, spasmolitic- and antianaphylactic activities [14-16]. The current interest in 2-amino-4H-chromene derivatives arises from their potential application in the treatment of human inflammatory TNFα-mediated diseases, such as psoriatic arthritis and rheumatoid and in cancer therapy [17]. Many of the methods reported for the synthesis of these compounds [18-21] are associated with the use of toxic catalyst and bases, long reaction time, and lack of general applicability. Thus, development of an efficient, facile, and clean method for the synthesis of chromene derivatives remains an issue of interest.

During the late several decades, Sonochemistry has gained increasing attention in chemistry research fields. The use of Sonochemical method as a green and significant technique, has many beneficial effects in synthetic organic chemistry and so organic chemists are focusing on its use for the synthesis of organic compounds. [22-24].

Considering the basic green chemistry concepts, ultrasound technique is proving to be more efficient and selectivity for improving the traditional reactions that require longer reaction time, unsatisfactory yields, expensive reagents and high temperatures [25,26].

U.S. irradiation offers an alternative energy source which is ordinarily accomplished by heating [27]. Ultrasound-assisted reactions proceed by acoustic cavitation phenomenon, that is, the formation, growth, and collapse of bubbles in the liquid medium [27].

During the collapse of a cavity, high local temperatures and pressures arise which lead to increase in the rate of reactions [28, 29].

In this study, we report magnetic Fe_3O_4-chitosan nanoparticles as a new magnetic nanocatalyst for the three-component synthesis of 2-amino-4*H*-chromenes under ultrasound irradiation (scheme 2). This green method is a rapid ultrasonic assisted route for the synthesis of wide variety of 2-amino-4*H*-chromenes.

< Scheme2>

2. Experimental

2.1. Chemical and apparatus

Chitosan (Medium molecular weight) was purchased from Aldrich company and used without any post-modification. Ferric chloride hexahydrate ($FeCl_3.6H_2O$, Merck), ferrous chloride tetrahydrate ($FeCl_2.4H_2O$, Merck), and chitosan (CS, Aldrich) were used as iron and polymer sources, respectively. All other chemical reagents in high purity were purchased from the Merck Chemical Company and used as received except for benzaldehyde which a fresh distilled sample was used. Melting points are determined in open capillaries using an Electrothermal Mk3 apparatus and are uncorrected. ^{1}H NMR and ^{13}C NMR spectra were recorded with a Bruker DRX-400 spectrometer at 400 and 100 MHz respectively. NMR spectra were reported as parts per million (ppm) downfield from tetramethylsilane as internal standard. The abbreviations used are: singlet (s), doublet (d), triplet (t) and multiplet (m). FT-IR spectra were obtained with potassium bromide pellets in the range 400–4000 cm^{-1} with a Perkin–Elmer 550 spectrometer. The elemental analysis (C, H, N) were obtained from a Carlo ERBA Model EA 1108 analyzer carried out on Perkin–Elmer 240c analyzer. The UV–vis measurements were obtained with a GBC cintra 6 UV–vis spectrophotometer. Nanostructures were characterized using a Holland Philips Xpert X-ray powder diffraction (XRD) diffractometer (CuK, radiation, k = 0.154056 nm), at a scanning speed of 2°/min from 10° to 100° (2ɵ). Scanning electron microscope characterization (SEM) was performed on a

FEI Quanta 200 SEM operated at a 20 kV accelerating voltage. The samples for SEM were prepared by spreading a small drop containing nanoparticles onto a silicon wafer and being dried almost completely in air at room temperature for 2 h, and then were transferred onto SEM conductive tapes. For conventional imaging in the SEM, specimens must be electrically conductive, at least at the surface, and electrically grounded to prevent the accumulation of electrostatic charge at the surface. So, the transferred sample was coated with a thin layer of gold before measurement. Sonication was performed in Shanghai Branson-BUG40-06 ultrasonic cleaner (with a frequency of 35 kHz and a nominal power 200 W) estimated calorimetrically. A circulating water bath (DC2006, Shanghai Hengping Apparatus Factory) with an accuracy of 0.1 K was adopted to keep the reaction temperature constant.

2.2 *preparation of magnetic heterogeneous catalyst*

Fe_3O_4 nanoparticles were prepared by chemical co-precipitation as described in the literature [30] and subsequently were functionalized with chitosan [31]. In short, 0.02 mol of $FeCl_3.6H_2O$ and 0.01 mol of $FeCl_2.4H_2O$ were dissolved in 80 mL of deionized water. Then, 10 mL of NH_4OH solution was added into the mixture at 80 ˚C under N_2 atmosphere and the black magnetic Fe_3O_4 nanoparticles were formed. Next, the reaction mixture was cooled and the catalyst was isolated in the magnetic field and washed three times with distilled water. Subsequently, In order prepare Fe_3O_4-chitosan nanoparticles, 1 g of the Fe_3O_4 nanoparticles was dispersed in 120 mL distilled water under ultrasound irradiation and 0.5 g of chitosan in 120 mL of 2.0 wt% acetic acid solution was slowly added under vigorous stirring at 50 ˚C for 1 h. The modified Fe_3O_4-chitosan nanoparticles were recovered by magnetic decantation and washed with CH_2Cl_2.finally, Fe_3O_4-chitosan nanoparticles were dried at 60 ˚C (Scheme 3).

< Scheme3>

2.3. *General procedure for the synthesis of 2-amino-4H-chromenes in water under silent condition*

A mixture of aldehyde (1 mmol), malononitrile (1 mmol), resorcinol (1 mmol) and Fe_3O_4-chitosan (0.15 g, 30 mol%) in water (5 mL) was taken in a 25 mL flask and the mixture was stirred under reflux conditions. After the completion of the reaction (monitored by TLC), the reaction was allowed to cool and the magnetic catalyst was removed by an external magnet. Then, the solvent was evaporated and the solid residue was recrystallized from ethanol to produce the product 4a in 89% yield.

2.4. *General procedure for the synthesis of 2-amino-4H-chromenes in water under ultrasound irradiation*

A 50 mL Erlenmeyer flask was charged with benzaldehyde (1 mmol), malononitrile (1 mmol), resorcinol (1 mmol) and Fe_3O_4-chitosan (0.15 g, 30 mol%) in water (5 mL). The reaction flask was taken in the ultrasonic bath, where the level of the reaction mixture is lower than the surface of the water. Then, the mixture was sonicated under 20, 40, 60, 80, and 100% of power of the ultrasonic bath at 50 °C for the appropriate time, as shown in Table 1. After the completion of the reaction (monitored by TLC), the reaction was allowed to cool and the magnetic catalyst was removed by an external magnet. Then, the solvent was evaporated and the solid residue was recrystallized from ethanol to afford the pure 2-amino-4*H*-chromene derivatives as white solid (Table 1).

< Table 1>

2.5. Spectral data for selected compounds

*2-5-1. 2-Amino-3-cyano-7-hydroxy-4-(3-hydroxyphenyl)-4H-chromene (**4e**)*

IR (KBr) (ν_{max} cm^{-1}): 3413 (OH), 3332 (NH_2), 2190 (CN), 1653 (C=C vinyl nitrile), 1587 (C=C aromatic); ^{1}H NMR (400 MHz, DMSO-d_6) δ: 4.51 (s, 1H, H-4), 6.42 (d, 1H, J=3 , H-Ar), 6.49 (dd, 1H, J=3, J=9, H-Ar), 6.54 (d, 1H, J=9, H-Ar), 6.86 (s, 2H, NH_2), 6.52-7.10 (m,

4H, H-Ar), 9.35 (s,1H, OH), 9.69 (s, 1H, 7-OH) ppm; ^{13}C NMR (100 MHz, DMSO-d_6) δ: 57.10, 102.56, 112.76, 112.99, 114.35, 114.50, 121.29, 126.48, 128.91, 129.96, 130.48, 138.93, 149.21, 157.43, 158.47, 160.59 ppm. Anal. Calcd. for. $C_{16}H_{12}N_2O_3$: C, 68.57; H, 4.32; N, 9.99%. Found: C, 68.53; H, 4.27; N, 9.92%.

*2-5-2. 2-Amino-3-cyano-7-hydroxy-4-(2,4-dichlorophenyl)-4H-chromene (**4h**)*

IR (KBr) (ν_{max} cm^{-1}): 3473 (OH), 3344 (NH_2), 2195 (CN), 1641 (C=C vinyl nitrile), 1594 (C=C aromatic); ^{1}H NMR (400 MHz, DMSO-d_6) δ: 5.15 (s, 1H, H-4), 6.41 (d, 1H, J=3, H-Ar), 6.47 (dd, 1H, J=9, J=3 , H-Ar), 6.72 (d, 1H, J=9 , H-Ar), 6.93 (s, 2H, NH_2), 7.23 (d, 1H, J=8 , H-Ar), 7.39 (dd, 1H, J=2, J=8, H-Ar), 7.62 (d, 1H, J=2 , H-Ar), 9.81 (s, 1H, OH) ppm; ^{13}C NMR (100 MHz, DMSO-d_6) δ: 56.64, 102.73, 112.72, 112.95, 113.87, 113.99, 121.12, 121.67, 129.79, 129.99, 130.34, 142.06, 149.38, 155.65, 159.96, 160.66 ppm. Anal. Calcd. for. $C_{16}H_{10}Cl_2N_2O_2$: C, 57.68; H, 3.03; N, 8.41%. Found: C, 57.8; H, 3.09; N, 8.45%.

*2-5-3. 2-Amino-3-cyano-7-hydroxy-4-(3,5-dimethoxyphenyl)-4H-chromene (**4j**)*

IR (KBr) (ν_{max} cm^{-1}): 3465 (OH), 3332 (NH_2), 2195 (CN), 1644 (C=C vinyl nitrile), 1629 (C=C aromatic); ^{1}H NMR (400 MHz, DMSO-d_6) δ: 3.68 (s, 6H, OMe), 4.56 (s, 1H, H-4), 6.29 (d, 1H, J=3 , H-Ar), 6.38 (dd, 1H, J=3, J=9, H-Ar), 6.49 (d, 1H, J=9 , H-Ar), 6.86 (s, 2H, NH_2), 6.99-7.29 (m, 3H, H-Ar), 9.76 (s, 1H, OH) ppm; ^{13}C NMR (100 MHz, DMSO-d_6) δ: 55.67, 56.49, 102.79, 112.75, 113.84, 121.08, 128.65, 129.66, 130.28, 131.10, 143.17, 149.18, 156.67, 159.81, 160.73 ppm. Anal. Calcd. for. $C_{18}H_{16}N_2O_4$: C, 66.66; H, 4.97; N, 8.64%. Found: C, 66.59; H, 4.94; N, 8.57%.

*2-5-4. 2-Amino-3-cyano-7-hydroxy-4-(2-furyl)-4H-chromene (**4l**)*

IR (KBr) (ν_{max} cm^{-1}): 3479 (OH), 3419 (NH_2), 2198 (CN), 1655 (C=C vinyl nitrile), 1586 (C=C aromatic); ^{1}H NMR (400 MHz, DMSO-d_6) δ: 4.77(s, 1H, H-4),), 6.18 (d, 1H, J=2 , H-Ar), 6.36 (dd, 1H, J=2, J= 8, H-Ar), 6.55 (d, 1H, J=8, H-Ar), 6.98 (s, 2H, NH_2), 7.28-7.55 (m, 3H, H-furyl), 9.77 (s, 1H, OH) ppm; ^{13}C NMR (100 MHz, DMSO-d_6) δ: 53.87, 102.87,

106.79, 110.33, 112.36, 112.98, 116.36, 120.93, 130.34, 149.57, 151.44, 155.58, 157.63, 161.37 ppm. Anal. Calcd. for. $C_{14}H_{10}N_2O_3$: C, 66.14; H, 3.96; N, 11.02%. Found: C, 66.09; H, 4.02; N, 11.05%.

*2-5-5. 2-Amino-3-cyano-7-hydroxy-4-(propyl)-4H-chromene (**4p**)*

IR (KBr) (ν_{max} cm^{-1}): 3467 (OH), 3333 (NH_2), 2196 (CN), 1644 (C=C vinyl nitrile), 1627 (C=C aromatic); ^{1}H NMR (400 MHz, DMSO-d_6) δ: 0.74 (t, 3H, Me), 1.07 (m, 2H, CH_3CH_2), 1.50 (m, 2H, CH_2CH), 3.36 (t, 1H, H-4), 6.34 (d, 1H, J=2, H-Ar), 6.53 (dd, 1H, J=2, J=10, H-Ar), 6.67 (s, 2H, NH_2), 6.90 (d, 1H, J=10, H-Ar), 9.58 (s, 1H, OH) ppm; ^{13}C NMR (100 MHz, DMSO-d_6) δ: 26.44, 26.67, 27.62, 43.81, 102.74, 107.99, 111.45, 112.24, 114.61, 121.61, 131.81, 156.62, 160.99 ppm. Anal. Calcd. for. $C_{13}H_{14}N_2O_2$: C, 67.81; H, 6.13; N, 12.17%. Found: C, 67.94; H, 6.17; N, 12.23%.

3. Results and discussion

3.1. Characterization of magnetic Fe_3O_4-chitosan nanoparticles as heterogeneous catalyst

Magnetic nanoparticles were synthesized by co-precipitation. Fig. 1a and 2a demonstrates crystal structures of Fe_3O_4 and Fe_3O_4-chitosan. The XRD patterns of Fe_3O_4 and Fe_3O_4-chitosan nanoparticles indicates iron oxide cubic structure and six peaks that related to the (220), (311), (400), (331), (422), (333), (440) and (531) planes. The weaker diffraction lines of magnetic Fe_3O_4-chitosan nanoparticles exhibite that the Fe_3O_4 nanoparticles were coated by amorphous chitosan polymer. But, chitosan did not destroy the crystal structure of iron oxide nanoparticles. The average crystal size of pure Fe_3O_4 and chitosan-coated Fe_3O_4 nanoparticles are 15 and 19, respectively.

< Fig. 1>

The SEM image (Fig. 2a) shows that magnetite Fe_3O_4 nanoparticles have a mean diameter of about 18 nm and Fig. 2(b) shows that magnetic Fe_3O_4-chitosan nanoparticles with nanometer size were successfully prepared and still keep the morphological properties of Fe_3O_4 except for a slightly larger particle size, which chitosan molecule is uniform coated on the Fe_3O_4 particles to form chitosan shell. Therefore, magnetic Fe_3O_4-chitosan nanoparticles have larger particle size than Fe_3O_4 nanoparticles. The SEM image shown in Fig. 2(b) demonstrates that the structure of Fe_3O_4-chitosan nanoparticles is looser, leading to the bigger size, the diameter of such a structure is more than 20 nm in size. So, it revealed the coating process and change in size of the particles.

< Fig. 2>

The elemental compositions are calculated from the energy dispersive X-ray (EDX). The elemental compositions of Fe_3O_4-chitosan nanoparticles are 74.6, 21.94, 2.94 and 0.52% for Fe, O, C, and N, respectively. This meant the chitosan was coated onto the surface of the Fe_3O_4 nanoparticles (Fig. 3).

< Fig. 3>

Fig 4 shows the fourier transform infrared (FT-IR) spectra of pure Fe_3O_4 nanoparticles (a), chitosan (b) and Fe_3O_4-chitosan (c). The characteristic peaks of Fe_3O_4 at 570 and 580 cm^{-1} could be observed in both (a) and (c). Also, the O-H streching vibration near 3423 cm^{-1} and 3430 cm^{-1} were observed in Fig. 4(a) and (c), which identifies these nanoparticles as Fe_3O_4 nanoparticles. The IR spectrum of chitosan was characterized by the following absorption bands: the (C-H) of backbone polymer appearing at 2874 and 2940 cm^{-1}; (C-O) of primary alcoholic group at 1424 cm^{-1}; and (N-H) at 3435 and 1653 cm^{-1}. Compared with the IR spectra of three samples (a, b, c), the presence of chitosan shifted the vibration of Fe_3O_4. The band shift of Fe-O stretching (from 570 to 580 cm^{-1}) and of N-H bending vibration from 1623 to 1630 cm^{-1} are the most significant, indicating that iron ions bind to the NH_2 group of

chitosan. Electrostatic interaction between the negatively charged Fe_3O_4 nanoparticles surface and the positively protonated chitosan also donates to the IR change. The peak at 3430 cm^{-1}in was probably attributed to the amino group of chitosan, which is overlapped by the O-H stretching vibration of Fe_3O_4 nanoparticles.

Thus, the magnetite nanocatalyst is stable during synthesis of 2-amino-4H-chromene in aqueous media.

< Fig. 4>

The magnetization curve for Fe_3O_4 nanoparticles and Fe_3O_4-chitosan nanoparticles is shown in Fig 5. Room temperature specific magnetization (M) versus applied magnetic field (H) curve measurements of the Fe_3O_4-chitosan nanoparticles indicate a saturation magnetization value (Ms) of 50.27 emu g^{-1}, lower than of pristine Fe_3O_4 nanoparticles (55.69 emu g^{-1}) due to the coated shell.

3.2. Evaluation of the catalytic activity of magnetic Fe_3O_4-chitosan nanoparticles through the synthesis of 2-amino-4H-chromenes.

To obtain appropriate conditions for the synthesis of 2-amino-4*H*-chromenes, different reaction conditions have been examined in the reaction of benzaldehyde 1a, resorcinol and malononitrile as a model reaction (Scheme 4).

< Scheme 4>

We investigated the effect of various solvents such as H_2O, EtOH, DMSO, DMF, CH_3CN, and CH_3Cl on a model reaction under ultrasound irradiation (power intensity: 80%) at 50 °C. The results were summarized in Table 2. Also, we tried the selected solvents under different power intensities. Although, the enhancement in the acoustic power could enhance the number of active cavitation bubbles and also the size of the individual bubbles, the model reaction showed the best yield in the presence of H_2O. It indicated that the role of solvent is more important than power intensity for this reaction.

< Table 2>

The best results were obtained using of 0.15 g (30 mol%) of Fe_3O_4-chitosan nanoparticles in H_2O (Table 2, Entry 1) of the corresponding product. Therefore H_2O was chosen as solvent of reaction. After this, the reaction was carried out in the presence of 0.05, 0.10, 0.15 and 0.20 g of Fe_3O_4-chitosan nanoparticles (Table 3) with and without sonication for the synthesis of 4a product.

< Table 3>

In all cases, the results shows that the reaction times are shorter and the yields of the products are higher under ultrasound irradiation. The reason may be the phenomenon of cavitation produced by ultrasound irradiation. Cavitation is the origin of sonochemistry, a physical process that creates, enlarges, and implodes gaseous and vaporous cavities in an irradiated liquid, therefore increasing the mass transfer and allowing chemical reactions to take place. Ultrasound wave propagates via an alternating adiabatic compression and rarefaction cycle waves induced in the molecules of the medium. In some cases, the rarefaction cycle may exceed the attractive forces of the molecules of the liquid at a sufficiently high power, which would involve a negative net pressure applied to the medium and consequently causing cavitation bubbles formation. This negative pressure can lead to rupture of the fluid and is accompanied by the generation of cavities. The varying pressure makes the bubbles oscillate in size. These oscillations are low energetic. Above a certain negative pressure threshold, this will lead to inertial cavitation, which is the high energetic fast growth and collapse of bubbles [33]. The bubbles are small can be seen as microreactors that offer the opportunity of speeding up certain reactions. Also, they allow mechanistically novel reactions to occur in an absolutely safe manner [23, 27, 34]. The use of 0.15 g of catalyst afforded the best yields under both conditions (Table 3, Entry 4). As shown in Table 3, in the absence of catalyst the yield of the 4a product was found to be low. In order to investigate the effect of intensity

power of ultrasonic on reaction, the reaction was carried out at 20%, 40%, 60%, 80% and 100% of the rate power of the ultrasonic bath (40, 80, 120, 160 and 200 W). The results are shown in Table 1. The intensity of sonication is proportional to the amplitude of vibration of the ultrasonic source and, as such, an increment in the amplitude of vibration will direct to an enhance in the intensity of vibration and to an enhance in the sonochemical effects. Increase of ultrasonic power led to higher yield and shorter reaction time before the ultrasound power intensity reached 80%, and then the yield decreased slightly with increasing ultrasound power intensity. Commonly, the enhance in the acoustic power could enhance the number of active cavitation bubbles and also the size of the individual bubbles. Both increases can be supposed to result in an increase in the maximum collapse temperature and the respective reaction could be did faster [35].

Different catalysts such as Fe_3O_4, chitosan and Fe_3O_4-chitosan nanoparticles were tested under ultrasound irradiation (Table 4). The reaction in the presence of Fe_3O_4-chitosan afforded the product in higher yield and shorter reaction time under ultrasound irradiation.

<Table 4>

2-amino-4*H*-chromenes was prepared by the wide range of substituted aldehydes under optimized reaction conditions in high to excellent yields (Table 5, method A).

< Table 5 >

Aldehydes bearing either electron-withdrawing or electron-donating groups showed equally well in the reaction and all 2-amino-4*H*-chromenes were prepared in high yields. For more examination of the effect of ultrasound irradiation in this reaction, comparison of the reaction under two methods, ultrasound irradiation at 50 °C (method A) and reflux conditions (method B) was carried out. As shown in Table 4, method A in comparison with method B is better in both yields and the reaction times.

A plausible mechanism explaining the aforementioned results and the selectivity is depicted in Scheme 5. The process represents a typical cascade of Knoevenagel condensation, Michael addition, and cyclization in the presence of Fe_3O_4-chitosan nanoparticles. As can be seen in Scheme 5, Fe_3O_4 as a lewis acid and the free hydroxyl groups on the surface of chitosan play a significant role in increasing the electrophilic character of the aldehyde and so can activate the carbonyl group of aldehyde 1a to decrease the energy of transition state for the nucleophilic attack of malononitrile. Also, lone pairs of amino group on surface of chitosan activate the nucleophilic property of the malononitrile. The reaction is thought to proceed through Knoevenagel condensation to form intermediate 5. Subsequently Michael addition occurs to form intermediate 6. The dipolar transition states (TS) occur resulting in generation intermediate of 6 in aqueous media as dipolar solvent that is converted to product 4a via an intramolecular cyclization. The mechanism of this reaction involves a polar transition state starting from a neutral ground state. ionic reactions are accelerated by physical effects better mass transport under ultrasonic irradiation. Generally, when ultrasound is passed through a liquid–solid system, bubble cavitation causes a series of unique physical phenomena that can affect the solid. Microjets and high energetic shockwaves are produced by inertial cavitation. Shockwaves are formed when cavities rapidly expand or collapse. Spherical particles can be accelerated significantly by the shockwave that occurs during the explosive growth of a cavity on the particle surface. During the collapse of a cavity, high local temperatures and pressures arise which result in a pressure shockwave. Shockwaves may cause mechanical damage to close objects and are known to cause material erosion. The collapse of bubbles close to a large rigid boundary will be asymmetric and leads to microjet formation in the direction of the surface. Microjets have an estimated speed of 100 m/s [aqueous solution; Suslick et al. (1990)] and lead to pitting and erosion of solid surface and the overall particle size reduction in heterogeneous systems. In fact, asymmetric collapse of the bubbles in heterogeneous system produce micro-jet with high velocity enhancing mass and heat transfer through stationary film surrounding adsorbent and also within the pores [36-40]. This effect is equivalent to high-pressure/high-velocity liquid jets. The jets activate the solid catalyst and enhance the mass transfer to the surface by the disruption of the interfacial boundary layers as well as dislodging the material occupying the inactive sites. Also, ultrasound irradiation can increase the surface area between the two phases for the reaction and provide additional activation through efficient mixing and improved mass transport, thus increasing the rate of the reaction. In addition, ultrasound irradiation activates the reaction mixture via inducing high local temperatures and pressure generated inside the cavitation bubble when it collapses

and increase the speed of the reaction rate [24]. Therefore, it is reasonable to assume that these effects should accelerate this reaction.

< Scheme 5>

The reusability is one of the important properties of this catalyst. After the completion of the reaction, ethyl acetate was added and the catalyst was separated by an external magnet. The catalyst was then washed with ethyl acetate, air-dried and used directly with fresh substrates under identical conditions without further purification. It was found that the catalyst could be reused for the next cycle without any appreciable loss of its activity. Similarly, reusability for sequential reaction was also carried out and catalyst was found to be reusable for four cycles (Table 5).

<Table 5>

The XRD of the recovered magnetic nanocatalyst was indexed according to the magnetite phase (Fig. 6), and so there is no considerable change in its magnetic phase. Therfore, the nanocatalyst is stable during synthesis of 2-amino-4*H*-chromenes under ultrasound irradiation.

<Fig. 6>

4. Conclusions

We have reported a green, efficient and environmentally procedure for the synthesis of 2-amino-4*H*-chromenes via condensation of various aldehydes with malononitrile and resorcinol using Fe_3O_4-chitosan nanoparticles as a magnetic heterogenous catalyst under ultrasound irradiation. This novel method offers several advantages including ease of separation and recovery, higher yields, safety, mild reaction conditions, short reaction time, simple workup procedure and recyclability of the magnetic nanocatalyst, as well as the ability to tolerate a large range of substitutions in the reagents**.**

Acknowledgements

We gratefully acknowledge the financial support from the Research Council of the University of Kashan for supporting this work by Grant NO. 256722/ XIII.

References

[1] N. D. Cuong, T. T. Hoa, D. Q. Khieu, T. D. Lam, N. D. Hoa, N. V. Hieu, J. Alloys Compd. 523 (2012) 120–126.
[2] A. H. Lu, E.L. Salabas, F. Schuth, Angew. Chem. Int. Ed. 46 (2007) 1222-1244.
[3] B. Hu, J. Pan, H.L.Yu, J.W.Liu, J.H. Xu, Process Biochem. 44 (2009)1019-1024.
[4]C.S. Gill, B.A. Price, C.W. Jones,J.Catal.251 (2007)145-152.
[5] Ataher, J.B. Kim, J.Y. Jung, W.S. Ahn, M.J. Jin, Synlett. (2009) 2477-2482.
[6] O.C. Dalaigh, a.S. Corr, Y. Gun Ko, J.S. Connon, Angew. Chem. Int. Ed. 46 (2007)4329-4332.
[7] Y. Zhang, Y. Zhao, C. Xia, J. Mol. Catal. A: Chem. 306 (2009) 107-112.
[8] A. Dong, Sh. Lan, J. Huang, T. Wang, T. Zhao, L. Xiao, W. Wang, X. Zheng, F. Liu, G. Gao,Y. Chen, ACS Appl. Mater. Interfaces, 3 (2011), 4228-4235.
[9] Lek, J.Y.,Xi, L., Kardynal, B.E., Wong, L.H., Lam, Y.M. ACS Appl. Mter. Interfaces 3 (2011) 287-292.
[10] H.V. Tran, L.D. Tran, T.N. Nguyen, Mater. Sci. Eng. C 30 (2010) 304–310.
[11] L.D. Tran, B.H. Nguyen, N.V. Hieu, H.V. Tran, H.L. Nguyen, P.X. Nguyen, Mater. Sci. Eng. C 31 (2011) 477–485.
[12] A. Shaabani and A. Maleki, *Appl. Catal.: A.*, 331 (2007) 149-151.
[13] M. G. Dekamin, M. Azimoshan and L. Ramezani, Green Chem.**,** 15 (2013) 811-820.
[14] M. S. Singh, S. Chowdhury, RSC Adv. 2012, 2, 4547-4592.
[15] G. Zhang, Y. Zhang, J. Yan, R. Chen, S. Wang, Y. Ma, R. Wang, J. Org. Chem. 77 (2012) 878-888.
[16] N. M. Sabry, H. M. Mohamed, E. S. A. E. H. Khattab, S. S. Motlaq, A. M. El-Agrody, Eur. J. Med. Chem. 46 (2011) 765-772.
[17] D. Wlodkowic, J. Skommer, M. Mättö, M. Eray, J. Pelkonen, Leuk. Res. 30 (2006) 322-331.
[18] G. Yang, C. Luo, X. Mu, T. Wang, X.-Y. Liu, Chem. Commun. 48 (2012) 5880-5882.
[19] S. Makarem, A. A. Mohammadi, A. R. Fakhari, Tetrahedron Lett. 49 (2008) 7194-7196.
[20] A. Shaabani, R. Ghadari, S. Ghasemi, M. Pedarpour, A. H. Rezayan, A. Sarvary, S. W. Ng, J. Comb. Chem. 11 (2009) 956-959.
[21] J. M. Khurana, B. Nand, P. Saluja, Tetrahedron 66 (2010) 5637-5641.
[22] J. Safari, M.N, Arani, Ultrason Sonochem. 18 (2011) 640-643.
[23] J. Safari, S.H. Banitaba, Sh. Dehghan Khalili, Ultrason Sonochem. 19 (2012) 1061–1069.
[24] J. Safari, S.H. Banitaba, S. D. Khalili, Ultrason. Sonochem. (2012), Ultrason. Sonochem. 20 (2013) 401–407.
[25] N.G. Khaligh, F. Shirini, Ultrason. Sonochem. 20 (2013) 19-25.
[26] N.G. Khaligh, F. Shirini, Ultrason. Sonochem. 20 (2013) 26–31.
[27] D. Nagargoje, P. Mandhane, S. Shingote, P. Badadhe, C. Gill, Ultrason. Sonochem. 19 (2012) 94–96.
[28] P. V. Shinde, B. B. Shingate, M. S. Shingare, Bull. Korean Chem. Soc. 32 (2011) 1179-1182.
[29] F. Dang, N.Y. Enomoto, J.C. Hojo, K.J. Enpuku, Ultrason Sonochem. 16 (2009) 649-654.
[30] J. Safari, L. Javadian, C. R. Chimie, 16 (2013), 1165-1171.
[31] N. D. Cuong, T. T. Hoa, D. Q. Khieu, T. D. Lam, N. D. Hoa, N. V. Hieu, J. Alloys Compd. 523 (2012) 120–126.
[32] J. Safari, Z. Zarnegar, M. Heydarian, Bull. Chem. Soc. Jpn. 85 (2012) 1332-1338.

[33] R.M. Wagterveld, L. Boels, M.J. Mayer , G.J. Witkamp Ultrason. Sonochem. 18 (2011) 216–225.
[34] D. Nagargoje, P. Mandhane, S. Shingote, P. Badadhe, C. Gill, Ultrason. Sonochem. 19 (2012) 94–96.
[35] X. Wang, Y. Wei, J. Wang, W. Guo, C. Wang, Ultrason. Sonochem. 19 (2012) 32–37.
[36]. R.M. Wagterveld ,L. Boels, M.J. Mayer a, G.J. Witkamp Ultrason. Sonochem. 18 (2011) 216–225.
[37] J. S. Markovski, V. Dokic´, M. Milosavljevic´, M. Mitric´, Aleksandra, A. Peric´-Grujic´, A. E. Onjia a, A. D. Marinkovic, Ultrason. Sonochem. 21 (2014) 790–801.
[38] L. H. Thompson, L. K. Doraiswamy Ind. Eng. Chem. Res. 38 (1999) 1215-1249.
[39] P. R. Gogate, V. S. Sutkar, A. B. Pandit, Chem. Eng. J. 166 (2011) 1066–1082.
[40] A. Ziarati, J. Safaei-Ghomi, S. Rohani, Ultrason. Sonochem. 20 (2013) 1069-1075.

Figures and captions

Scheme1. Chemical structure of chitosan

Scheme2. One-pot synthesis of 2-amino-4*H*-chromenes catalyzed by Fe_3O_4-chitosan nanoparticles.

under ultrasound irradiation at 50 °C.

Scheme 3. Synthesis of Fe_3O_4-chitosan nanoparticles.

Scheme 4. Standard model reaction.

Scheme 5. The plasuable mechanism for one-pot synthesis of 2-amino-4*H*-chromenes

Fig. 1. XRD pattern of Fe_3O_4 (a) and chitosan-coated Fe_3O_4 (b).

Fig. 2. SEM images of Pure Fe_3O_4 (a) and chitosan-coated Fe_3O_4(b)**.**

Fig. 3. The energy dispersive X-ray (EDX) of Fe_3O_4-chitosan nanoparticles.

Fig. 4. FT-IR of spectra of pure Fe_3O_4 nanoparticles (a), chitosan (b) and Fe_3O_4-chitosan (c).

Fig. 5. Magnetization versus applied field (H) isotherms for Fe_3O_4 nanoparticles and chitosan-coated Fe_3O_4.

Fig. 6. XRD patterns of recovered Fe_3O_4-chitosan nanoparticles after five recovery.

Table 1. The effect of intensity power of ultrasonic on the synthesis of 4a.[a]

Table 2. Optimization of reaction conditions for synthesis of **4a** under ultrasound irradiation.[a]

Table 3. Comparison of yield and reaction time with or without ultrasound irradiation for the synthesis of **4a** product.

Table 4. Screening of type of catalyst for the synthesis of 2-amino-4*H*-chromenes [a].

Table 5. Fe_3O_4-chitosan nanoparticles catalyzed three component condensations of malononitrile
aldehydes and resorcinol to form 2-amino-4*H*-chromenes under ultrasound irradiation.

Table 6. The effect of reusability of Fe_3O_4-chitosan nanoparticles on the product 4a yeild[a].

Table 1. The effect of intensity power of ultrasonic on the synthesis of 4a.[a]

Yield (%)	Time (min)	Max power/intensity (W)	Entry
72	29	20% (40 W)	1
75	25	40% (80 W)	2
76	22	60% (120 W)	3
99	20	80% (160 W)	4
86	21	100% (200 W)	5

[a]Reaction conditions: aldehyde **1a** (1 mmol), malononitrile **2** (1 mmol), resorcinol **3** (1 mmol), Fe_3O_4-chitosan nanoparticles (0.15 g, 30 mol%) and 5 ml water

Table 2. Optimization of reaction conditions for synthesis of **4a** under ultrasound irradiation.[a]

Yield[b] (%)	Time (min)	Method	Solvent	Entry
trace	35	Ultrasound	None	1
73	35	Ultrasound	Chloroform	2
77	35	Ultrasound	DMSO	3
86	35	Ultrasound	Acetonitrile	4
83	35	Ultrasound	DMF	5
92	25	Ultrasound	EtOH	6
99	20	Ultrasound	Water	7
90	31	High speed stirring	Water	8

[a] Reaction conditions: aldehyde **1a** (1 mmol), malononitrile **2** (1 mmol), and resorcinol **3** (1 mmol), catalyst (0.15 g, 30 mol%), 5 ml solvent under ultrasound irradiation at 50°C.
[b] Isolated yield.

Table 3 Comparison of yield and reaction time with or without ultrasound irradiation for the synthesis of **4a** product.

With sonication	Without sonication	Catalyst (g)	Entry
Yield (%) / Time (min)	Yield (%) / Time (min)		
82/30	71/65	0	1
87/25	78/47	0.05	2
88/23	85/49	0.10	3
99/20	90/31	0.15	4
99/20	90/31	0.20	5

[a] Reflux condition.

[b] Under ultrasonic waves (power intensity: 80%) at 50°C.

Table 4.

Screening of type of catalyst for the synthesis of 2-amino-4*H*-chromenes [a].

Yield (%)	Time (min)	Catalyst	Entry
82	30	None	1
98	24	Fe_3O_4	2
97	21	Chitosan	3
99	20	Fe_3O_4-chitosan	4

[a] Reaction conditions: aldehyde **1a** (1 mmol), malononitrile **2** (1 mmol), and resorcinol **3** (1 mmol), catalyst (0.15 g, 30 mol%), 5 ml solvent under ultrasound irradiation at 50°C.

Table 5. Fe_3O_4-chitosan nanoparticles catalyzed three component condensations of malononitrile aldehydes and resorcinol to form 2-amino-4*H*-chromenes under ultrasound irradiation.

m.p.$_{rep}$/m.p.$_{lit.}$ (°C)[b]	Time (min)/ Yield (%)[a]	Product	R	Entry
235-238/234-237	20/99	**4a**	C_6H_5	1
180-183/183-186	23/97	**4b**	4-MeC_6H_4	2
108-111/110-11112	25/94	**4c**	4-$MeOC_6H_4$	3
103-106/106-109	15/96	**4d**	3-ClC_6H_4	4
216-218/215-217	25/95	**4e**	3-HOC_6H_4	5
219-222/218-221	20/97	**4f**	2-FC_6H_4	6
224-227/222-224	27/95	**4g**	2-$MeOC_6H_4$	7
257-259/256-258	15/96	**4h**	2,4-$Cl_2C_6H_3$	8
219-221/217-220	15/95	**4i**	2,6-$Cl_2C_6H_3$	9
189-190/191-193	25/95	**4j**	3,5-$(MeO)_2C_6H_3$	10
230-232/230-232	20/95	**4k**	2-Naphthyl	11
209-211/208-210	15/97	**4l**	2-Furyl	12
230-232/228-231	15/96	**4m**	2-Thienyl	13
180-183/179-181	18/96	**4n**	5-Mefuryl	14
167-170/169-172	22/95	**4o**	Ethyl	15
163-166/160-162	23/97	**4p**	propyl	16
125-128/124-126	23/95	**4q**	Hepthyl	17
>300/>300	20/98	**4r**	$OHCC_6H_4$	18

[a] Isolated yields.

[b] ref [32]

Table 6. The effect of reusability of Fe_3O_4-chitosan nanoparticles on the product 4a yeild[a].

Yield (%)[b]	Cycle	Entry
99	0	1
99	1	2
98	2	3
97	3	4
97	4	5
92	5	6

[a] Reaction conditions: malononitrile (1 mmol), aldehyde **1a** (1 mmol) and resorcinol (1 mmol), Fe_3O_4-chitosan nanoparticles (0.15 g, 30 mol%) under U.S. irradiation.

[b] Isolated yields.

Scheme 1. Chemical structure of chitosan.

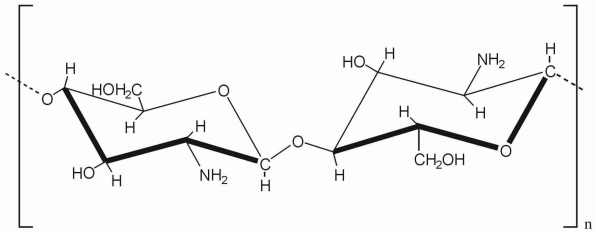

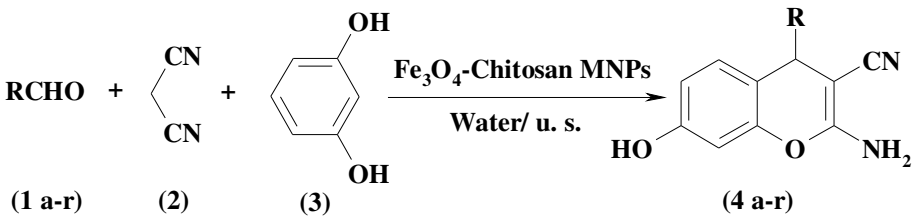

Scheme2. One-pot synthesis of 2-amino-4*H*-chromenes catalyzed by Fe_3O_4-chitosan nanoparticles under ultrasound irradiation at 50 ˚C.

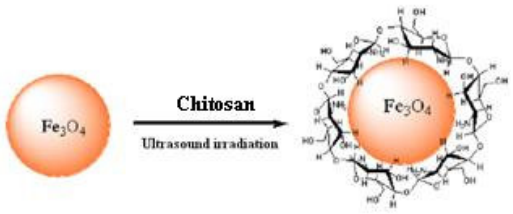

Scheme 3. Synthesis of Fe_3O_4-chitosan nanoparticles.

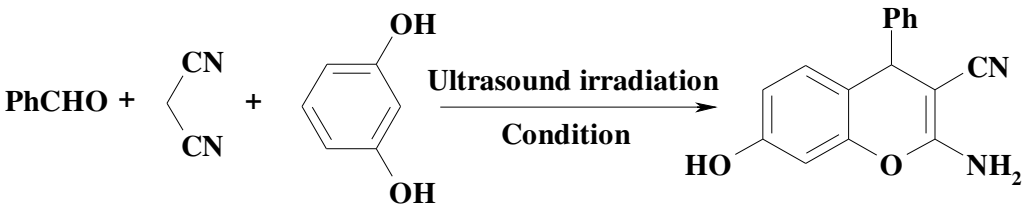

Scheme 4. Standard model reaction.

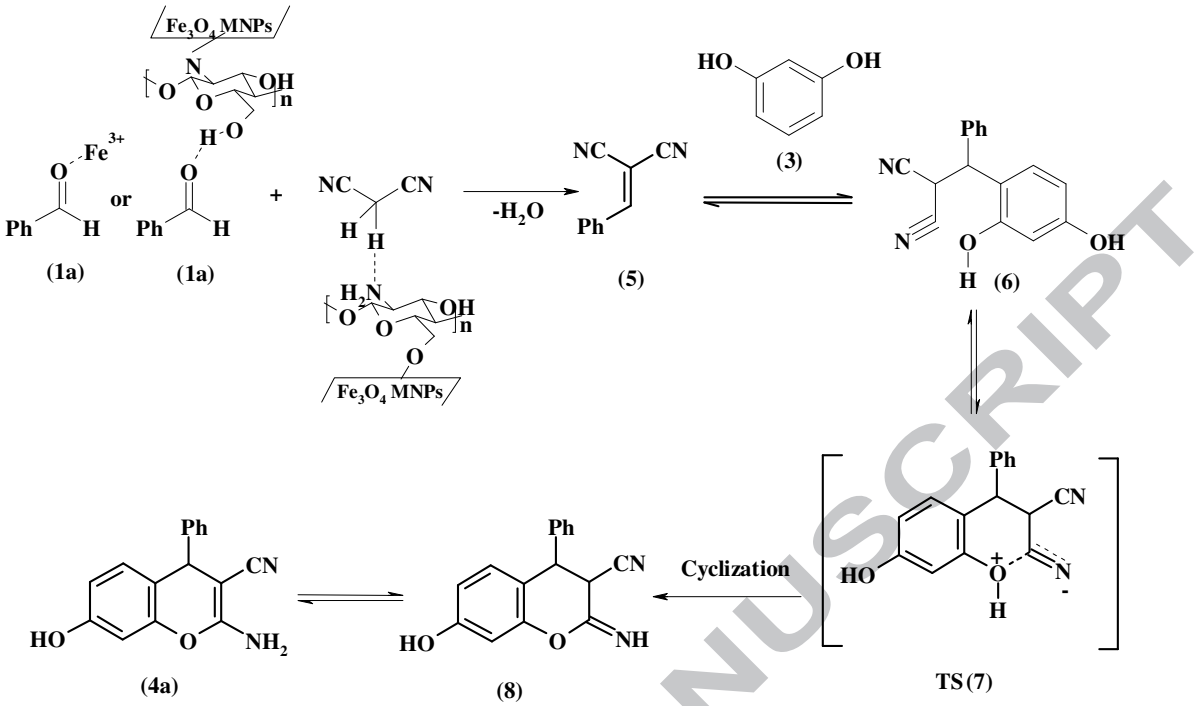

Scheme 5. The plasuable mechanism for one-pot synthesis of 2-amino-4*H*-chromenes

Fig. 1. XRD pattern of Fe_3O_4 (a) and chitosan-coated Fe_3O_4 (b).

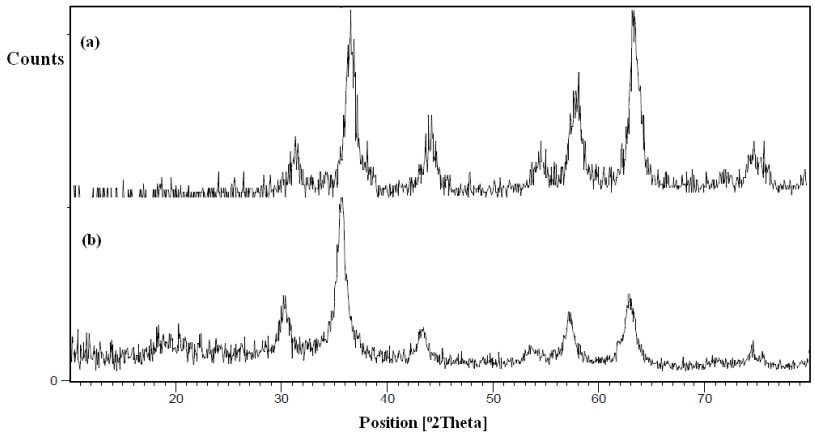

Fig. 2. SEM images of Pure Fe_3O_4 (a) and chitosan-coated Fe_3O_4(b)**.**

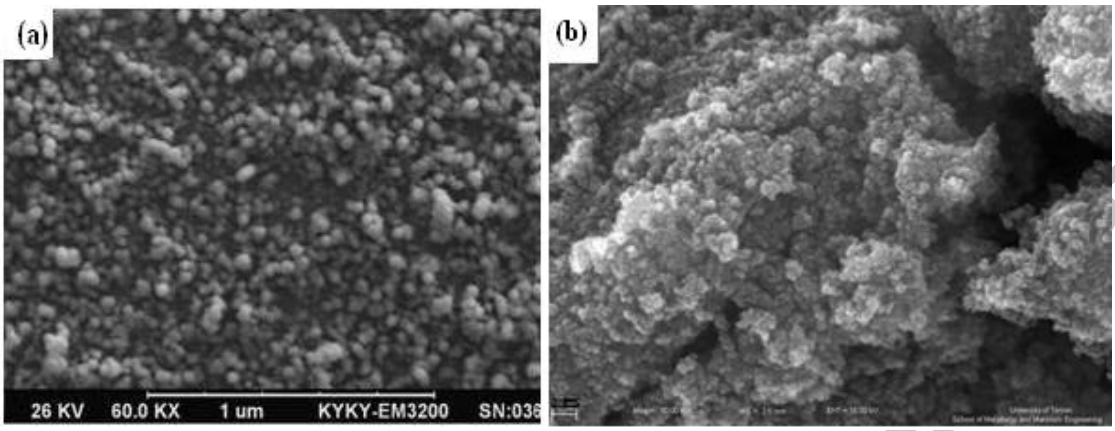

Fig. 3. The energy dispersive X-ray (EDX) of Fe_3O_4-chitosan nanoparticles.

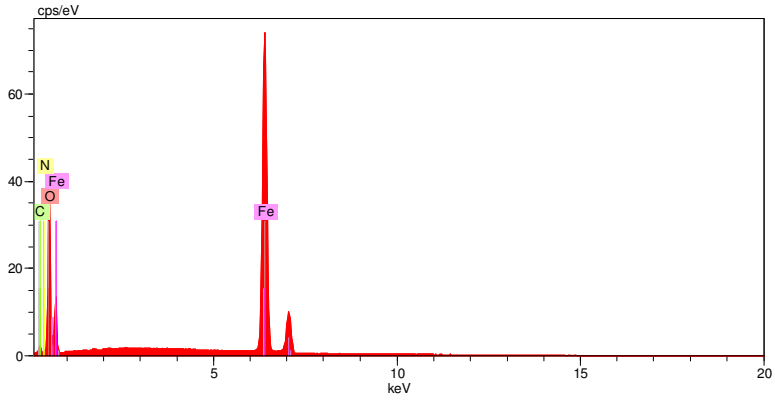

Fig. 4. FT-IR of spectra of pure Fe_3O_4 nanoparticles (a), chitosan (b) and Fe_3O_4-chitosan (c).

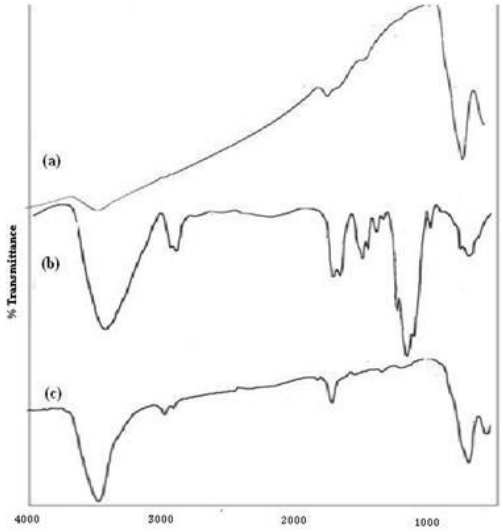

Fig. 5. Magnetization versus applied field (H) isotherms for Fe_3O_4 nanoparticles and chitosan-coated Fe_3O_4.

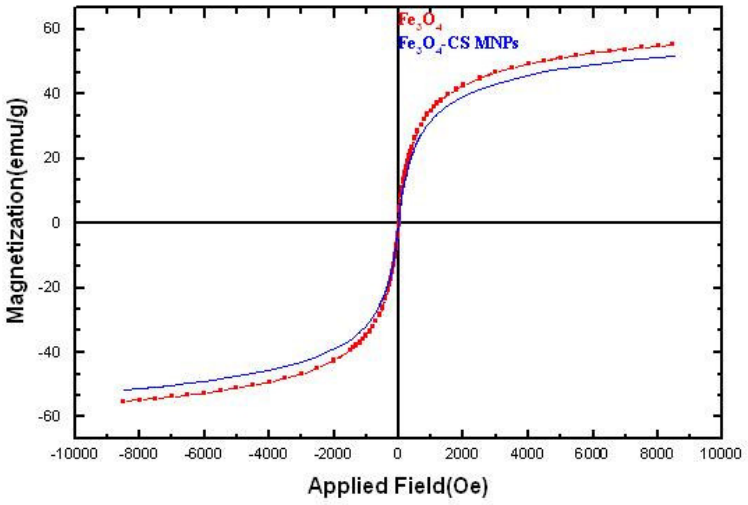

Fig. 6. XRD patterns of recovered Fe_3O_4-chitosan nanoparticles after four recovery.

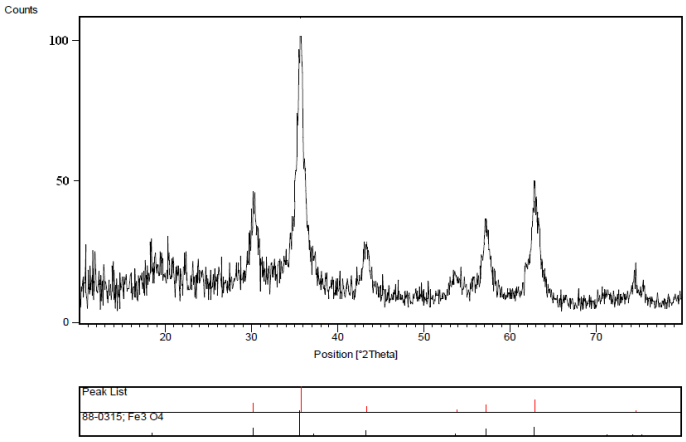

Tables:

Table 1. The effect of intensity power of ultrasonic on the synthesis of 4a.[a]

Entry	Max power/intensity (W)	Time (min)	Yield (%)
1	20% (40 W)	29	72
2	40% (80 W)	25	75
3	60% (120 W)	22	76
4	80% (160 W)	20	99
5	100% (200 W)	21	86

[a]Reaction conditions: aldehyde **1a** (1 mmol), malononitrile **2** (1 mmol), resorcinol **3** (1 mmol), Fe_3O_4-chitosan nanoparticles (0.15 g, 30 mol%) and 5 ml water

Table 2. Optimization of reaction conditions for synthesis of **4a** under ultrasound irradiation.[a]

Entry	Solvent	Method	Time (min)	Yield[b] (%)
1	None	Ultrasound	35	trace
2	Chloroform	Ultrasound	35	73
3	DMSO	Ultrasound	35	77
4	Acetonitrile	Ultrasound	35	86
5	DMF	Ultrasound	35	83
6	EtOH	Ultrasound	25	92
7	Water	Ultrasound	20	99
8	Water	High speed stirring	31	90

[a] Reaction conditions: aldehyde **1a** (1 mmol), malononitrile **2** (1 mmol), and resorcinol **3** (1 mmol), catalyst (0.15 g, 30 mol%), 5 ml solvent under ultrasound irradiation at 50°C.
[b] Isolated yield.

Table 3 Comparison of yield and reaction time with or without ultrasound irradiation for the synthesis of **4a** product.

Entry	Catalyst (g)	Without sonication	With sonication
		Yield (%) / Time (min)	Yield (%) / Time (min)
1	0	71/65	82/30
2	0.05	78/47	87/25
3	0.10	85/49	88/23
4	0.15	90/31	99/20
5	0.20	90/31	99/20

[a] Reflux condition.

[b] Under ultrasonic waves (power intensity: 80%) at 50°C.

Table 4.

Screening of type of catalyst for the synthesis of 2-amino-4*H*-chromenes [a].

Entry	Catalyst	Time (min)	Yield (%)
1	None	30	82
2	Fe_3O_4	24	98
3	Chitosan	21	97
4	Fe_3O_4-chitosan	20	99

[a] Reaction conditions: aldehyde **1a** (1 mmol), malononitrile **2** (1 mmol), and resorcinol **3** (1 mmol), catalyst (0.15 g, 30 mol%), 5 ml solvent under ultrasound irradiation at 50°C.

Table 5. Fe_3O_4-chitosan nanoparticles catalyzed three component condensations of malononitrile aldehydes and resorcinol to form 2-amino-4*H*-chromenes under ultrasound irradiation.

Entry	R	Product	Time (min)/ Yield (%)[a]	m.p.$_{rep.}$/m.p.$_{lit.}$ (°C)[b]
1	C_6H_5	**4a**	20/99	235-238/234-237
2	4-MeC_6H_4	**4b**	23/97	180-183/183-186
3	4-$MeOC_6H_4$	**4c**	25/94	108-111/110-11112
4	3-ClC_6H_4	**4d**	15/96	103-106/106-109
5	3-HOC_6H_4	**4e**	25/95	216-218/215-217
6	2-FC_6H_4	**4f**	20/97	219-222/218-221
7	2-$MeOC_6H_4$	**4g**	27/95	224-227/222-224
8	2,4-$Cl_2C_6H_3$	**4h**	15/96	257-259/256-258
9	2,6-$Cl_2C_6H_3$	**4i**	15/95	219-221/217-220
10	3,5-$(MeO)_2C_6H_3$	**4j**	25/95	189-190/191-193
11	2-Naphthyl	**4k**	20/95	230-232/230-232
12	2-Furyl	**4l**	15/97	209-211/208-210
13	2-Thienyl	**4m**	15/96	230-232/228-231
14	5-Mefuryl	**4n**	18/96	180-183/179-181
15	Ethyl	**4o**	22/95	167-170/169-172
16	propyl	**4p**	23/97	163-166/160-162
17	Hepthyl	**4q**	23/95	125-128/124-126
18	$OHCC_6H_4$	**4r**	20/98	>300/>300

[a] Isolated yields.

[b] ref [32]

Table 6. The effect of reusability of Fe_3O_4-chitosan nanoparticles on the product 4a yeild[a].

Entry	Cycle	Yield (%)[b]
1	0	99
2	1	99
3	2	98
4	3	97
5	4	97
6	5	92

[a] Reaction conditions: malononitrile (1 mmol), aldehyde **1a** (1 mmol) and resorcinol (1 mmol), Fe_3O_4-chitosan nanoparticles (0.15 g, 30 mol%) under U.S. irradiation.

[b] Isolated yields.

Highlights

► Ultrasonic-assisted green synthesis of 2-amino-4*H*-chromene derivatives.

► The effect of frequency of ultrasound irradiation on the reaction was surveyed.

►With simple precursors fe_3O_4-Chitosan nanoparticles were prepared under ultrasound irradiation.

► Using of both magnetic nanocatalyst and ultrasound irradiation for improvement of yields and reaction times than the reported methods